Bioorganic Chemistry 38 (2010) 98–107

Contents lists available at ScienceDirect

Bioorganic Chemistry

journal homepage: www.elsevier.com/locate/bioorg

An investigation into the N- and C-capping effects of glycine in cavitand-based four-helix bundle proteins

Heidi E.K. Huttunen-Hennelly *,[1]

Department of Chemistry, Thompson Rivers University, 900 McGill Road, PO Box 3010, Kamloops, BC, Canada, V2C 5N3

ARTICLE INFO

Article history:
Received 29 October 2009
Available online 25 January 2010

Keywords:
de novo protein
Protein design
Protein folding
Synthetic proteins
Four-helix bundle
Template assembled synthetic protein (TASP)
Helix capping

ABSTRACT

The capping efficiency of glycine on cavitand-based synthetic four-helix bundles was investigated. Glycine, a common C-capping amino acid, has always been included as a C-terminal residue in our *de novo* peptides, although the exact contribution of the glyince cap to the overall stability and structure of the caviteins had not previously been examined. The uncapped proteins were found to be less helical according to their CD spectra. In addition, the H/D exchange experiments suggested that the uncapped caviteins were more conformationally flexible. Capped and uncapped caviteins exhibited similar $\Delta G^{o}_{H_2O}$ values of unfolding. Overall, it can be concluded that glycine caps are useful, as they reduce helical unravelling and enhance helicity, and thus, glycine will be included as a C-terminal residue in future *de novo* peptide sequences.

1. Introduction

The design of new synthetic proteins in order to help elucidate the protein-folding problem has received great attention over the past few decades [1]. The use of templates to assist in the organization of peptides to form pre-determined three-dimensional structures, Template Assembled Synthetic Proteins (TASPs), has emerged as a useful tool in this area of research [2]. We covalently link α-helical peptides to a cavitand template, referring to the resulting structures as "*caviteins*" (*cavi*tand + pro*tein*) (Fig. 1) [3]. One of the advantages of *de novo* peptides is that they are generally smaller and more simple than their natural counterparts, yet they still maintain the same features necessary for folding. One of the most common topologies encountered among the examples of *de novo* proteins is the four-helix bundle [4]. In addition to providing models for understanding the challenges of the folding process, *de novo* proteins are novel molecules with potentially useful applications [5].

The α-helix contains internal hydrogen bonds between the carbonyl of residue *i* and the amide proton of residue *i* + 4 [6]. This network leaves four carbonyl groups at the C-terminus, and four amide protons at the N-terminus, without hydrogen bonding partners [7]. It has been proposed that there is a preference for certain residues to reside at the N- and C-termini of helices that will satisfy the hydrogen-bonding requirements and stabilize the helix macrodipole [7,8]. Amino acids having charged side chains that can minimize the helix macrodipole, created by the orientation of the amide residues of the helix backbone, are prevalent at the appropriate helix termini. For example, a cationic side chain can stabilize a helix if it is located at the negatively charged C-terminus, and an anionic side chain can stabilize the positively charged N-terminus.

The alternative hydrogen bonds that occur at helix N- and C-termini are termed helix "capping" interactions and provide thermodynamic stability to α-helices. N-caps have been shown to stabilize monomeric α-helices by up to 2 kcal/mol [9]. Amino acids that serve as useful N-caps include Ser, Asn, Asp and Thr, while Ala, Leu, Val, Ile, Trp, Arg, Gln and Glu are rarely found [7,8,10]. Ser, Asn, Asp and Thr are favourable N-caps because they can adopt specific rotameric conformations that allow for their side chains to accept hydrogen bonds from free main chain NH groups, thus stabilizing the α-helix.

By comparison, C-capping interactions occur less frequently than N-capping interactions of the α-helices in proteins of known structure, and it appears that C-capping motifs may be more important for helix termination than for stabilization [8]. Furthermore, the stabilizing effects of C-capping residues such as His, Lys and Arg were found to be much less (only ~0.3–0.6 kcal/mol of stabilization has been observed) than that of N-caps [9a]. The positively charged side chains of His, Lys, and Arg help stabilize the negatively charged C-terminus. However, the most common residue found at the C-cap position is glycine, a good helix terminating residue.

* Fax: +1 (250) 828 5450.
E-mail address: hhuttunen@tru.ca
[1] Research was completed at the University of British Columbia, Vancouver BC, Canada.

0045-2068/$ - see front matter © 2010 Elsevier Inc. All rights reserved.
doi:10.1016/j.bioorg.2010.01.004

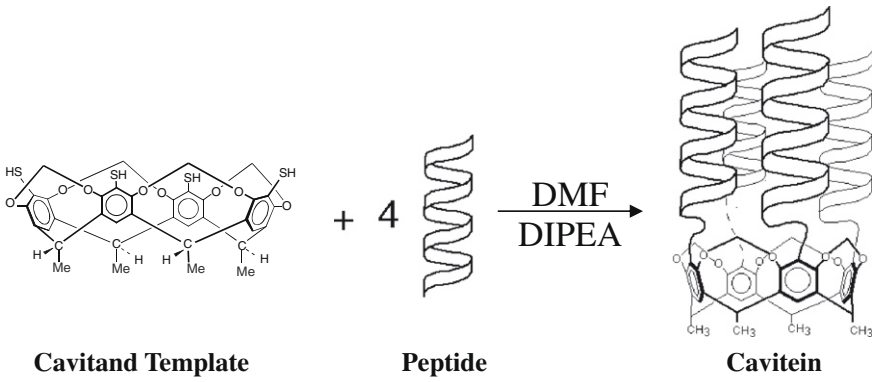

Fig. 1. Cavitein synthesis.

This study aimed at determining whether removing a glycine N- or C-cap would alter not only stability, as is commonly probed, but also the structure and dynamics of the resulting caviteins. It was hypothesized that caviteins containing peptides, with glycine caps, would be more helical, more stable, and less dynamic compared to their uncapped derivatives. A greater stability of ~1–2 kcal/mol, as is generally reported for proteins in literature [9], was predicted for caviteins containing peptides having glycine C-caps, and ~0.3–0.6 kcal/mol greater stability for caviteins containing peptides with N-caps. It is important to note that the changes in stability that were being evaluated were subtle. A crystal structure of a cavitein-dimer was recently reported by Sherman and co-workers, which shows a stabilizing glycine C-capping interaction, and hence it was interesting to evaluate the effect of glycine capping with respect to cavitein structure, dynamics and stability [3g]. The approach involved synthesizing caviteins having similar peptides linked to the cavitand template via their N- and C-termini, respectively. Furthermore, these caviteins were synthesized with and without glycine capping residues at their respective helix termini.

2. Results and discussion

2.1. Peptide synthesis

Peptides **1–6** were synthesized using standard Fmoc techniques on an automated Applied Biosystems peptide synthesizer following literature procedures; the sequences are outlined in Table 1 [11].

2.2. Cavitein synthesis

The synthesis of caviteins **7, 8, 10,** and **11** entailed the coupling of activated peptides **1**, **2**, **4,** and **5** to the cavitand template via their N-termini through disulfide bonds by following literature procedures [3b]. Caviteins **9** and **12** had peptides **3** and **6** linked to the cavitand via their C-termini, respectively, also by following literature procedures [12]. A complete list of the caviteins and their corresponding names are outlined in Table 2.

Table 1
Complete sequences using one-letter abbreviated amino acids including modified termini for peptides **1**–**6**.

Peptide number	Peptide name	Peptide sequence
1	lg2	$ClCH_2CO$–NH–[GG–EELLKKLEELLKKG]–CO–NH_2
2	lg3	$ClCH_2CO$–NH–[GGG–EELLKKLEELLKKG]–CO–NH_2
3[a]	lg2c	CH_3CO–NH–[GEELLKKLEELLKKGGC]–Spy
4	lg2_nocap	$ClCH_2CO$–NH–[GG–EELLKKLEELLKK]–CO–NH_2
5	lg3_nocap	$ClCH_2CO$–NH–[GGG–EELLKKLEELLKK]–CO–NH_2
6[a]	lg2c_nocap	CH_3CO–NH–[EELLKKLEELLKKGGC]–Spy

[a] lg2c is attached to the cavitand via a C-terminal cysteine residue; Spy is the S-pyridyl group.

2.3. Characterization

Caviteins **7–12** were synthesized with high levels of purity, and were characterized by circular dichroism (CD), nuclear magnetic resonance (NMR) spectroscopy, analytical ultracentrifugation (AUC), and by the binding of a hydrophobic dye, 1-anilinonaphthalene-8-sulfonate (ANS), monitored by fluorescence spectroscopy.

2.4. Far-UV CD spectroscopy

The far-UV CD spectra for the caviteins at concentrations of ~40 μM are shown in Fig. 2. CD spectra for each of the caviteins were also obtained at ~4 μM to evaluate whether concentration has an effect on the α-helicity of the protein. For all of the caviteins, the CD spectra at concentrations of ~4 and ~40 μM were indistinguishable; only the high concentration data is shown. The concentration independence supports that the proteins are monomeric at these concentrations.

The characteristic CD curves for all of the caviteins indicate an α-helical structure. The α-helicities of the uncapped caviteins in all cases are lower than their respective capped counterparts. The LG2C cavitein, which has its peptides linked to the template via their C-termini, seems to be the most helical of the six caviteins, while LG2C_nocap is the least helical.

2.5. Near-UV CD spectroscopy

The disulfide or aromatic chromophores absorb in the near-UV CD region, which provide information on the tertiary structures of proteins [13]. LG2C and LG2C_nocap have disulfide bonds which absorb in the near-UV region, as do all of the caviteins having the arenes in the cavitand template. The near-UV CD spectra for the capping caviteins at concentrations of ~40 μM are shown in Fig. 3.

The removal of the capping residues in LG2, LG3, and LG2C has little effect on the near-UV CD signal. The enhanced near-UV signal of LG2 and LG2_nocap could be a result of the peptides being located in closer proximity to the cavitand template, which is the chromophore in the near-UV region. From the patterns of the near-UV signals, it may be that LG2 and LG2_nocap are supercoiling in one direction, and in the opposite direction to that of LG3 and LG3_nocap. Furthermore, the absence of a CD signal in the

Table 2
Names and sequences for caviteins **7–12**.

Cavitein number	Cavitein name	Sequence
7	LG2	Cavitand–(S–CH_2CO–NH–[GG–EELLKKLEELLKKG]–CO–NH_2)$_4$
8	LG3	Cavitand–(S–CH_2CO–NH–[GGG–EELLKKLEELLKKG]–CO–NH_2)$_4$
9[a]	LG2C	Cavitand–(S–[CGG–KKLLEELKKLLEEG]–NH–$COCH_3$)$_4$
10	LG2_nocap	Cavitand–(S–CH_2CO–NH–[GG–EELLKKLEELLKK]–CO–NH_2)$_4$
11	LG3_nocap	Cavitand–(S–CH_2CO–NH–[GGG–EELLKKLEELLKK]–CO–NH_2)$_4$
12[a]	LG2C_nocap	Cavitand–(S–[CGG–KKLLEELKKLLEE]–NH–$COCH_3$)$_4$

[a] Caviteins 9 and 12 have peptides linked to the cavitand via their C-termini.

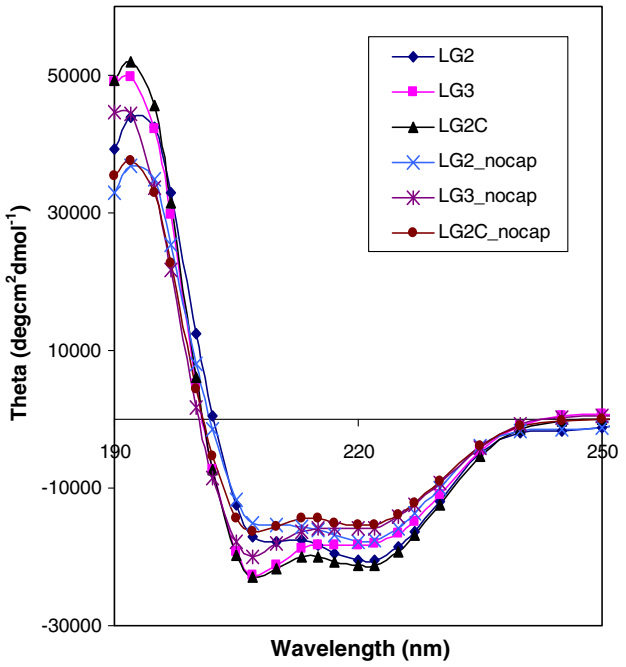

Fig. 2. Far-UV CD spectra for the caviteins at ~40 μM in 50 mM pH 7.0 sodium-phosphate buffer at 20 °C.

near-UV region for LG2C and LG2C_nocap suggest that either their chiral elements are removed from the cavitand chromophores or that they exhibit molten globule-like characteristics. The latter conclusion would be in accord with other disulfide-linked caviteins that also exhibited molten globule-like characteristics, previously studied [12] see Table 3.

2.6. GuHCl denaturation experiments

Fig. 4 displays the unfolding curves of the capping caviteins monitored at 222 nm in the presence of 0–8.0 M GuHCl at ~40 μM concentrations. The GuHCl experiments were also run at 4 μM concentrations for each of the caviteins. The unfolding curves at each concentration are superimposable within experimental error, reflected by their similar $\Delta G^{o}_{H_2O}$ values listed in Table 4.

The cooperativity of the unfolding reaction can be measured qualitatively by the width and shape of the unfolding transition. All of the unfolding curves for the caviteins shown in Fig. 4 show that: (1) the caviteins exist as well-folded structures before GuHCl

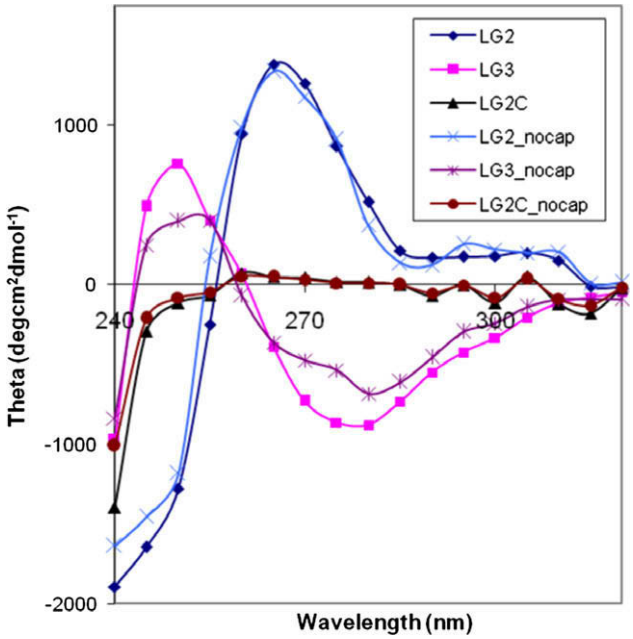

Fig. 3. Near-UV CD spectra for the caviteins at ~40 μM in 50 mM pH 7.0 sodium-phosphate buffer at 20 °C.

is added, (2) all the caviteins are completely unfolded by 8.0 M GuHCl, and (3) the unfolding transitions are cooperative.

Surprisingly, because it was predicted that the uncapped caviteins would be slightly less stable (~0.3–2 kcal/mol depending on the helix cap) than their capped analogues, the $\Delta G^{o}_{H_2O}$ values of unfolding for each capped/uncapped pair of caviteins fall within experimental error of each other.

2.7. AUC sedimentation equilibrium experiments

AUC sedimentation equilibrium experiments have been used to analyze the solution behaviour of various biological molecules [14]. The caviteins were analyzed at concentrations of 10, 50 and 80 μM and at rotor speeds of 27,000, 35,000 and 40,000 rpm. The sedimentation equilibrium data for the caviteins were analyzed by NONLIN [15], and the exponential plot of absorbance versus radius for LG2_nocap is shown in Fig. 5. The exponential plots of absorbance for LG3_nocap, and LG2C_nocap were very similar to that of LG2_nocap, (data not shown).

The data for each of the caviteins were fit to a monomer, monomer–dimer, dimer, monomer–trimer, trimer, monomer–tetramer, and tetramer in order to check for the best theoretical fit to the experimental data. In all cases the monomer fits were most accurate, assessed by the even distribution of the residuals about zero as exemplified in the upper panel of Fig. 5. Table 5 summarizes the sedimentation data, and the solution conditions for the caviteins.

2.8. One-dimensional ^{1}H NMR spectroscopy

The amide region of the ^{1}H NMR spectra for four of the caviteins is shown in Fig. 6. The ^{1}H NMR spectrum of LG2C_nocap could not be acquired due to insufficient sample quality. Sharp and disperse signals in the amide region are indicative of native-like structure [16].

The ^{1}H NMR spectra of LG2, LG2_nocap, LG3, and LG3_nocap each show ~13 distinguishable dispersed amide signals indicative of a well-defined amide backbone with a high content of tertiary

Table 3
Molar ellipticity at 222 nm ($[\theta]_{222}$) for the caviteins.

Cavitein	Concentration (μM)	Experimental $(\theta)_{222}$ (deg cm^2 dmol^{-1})	Calculated maximum $(\theta)_{222}$ (deg cm^2 dmol^{-1})	Percent helicity (%)
LG2[a]	39	~−20,000	~−33,200	~60
LG3[a]	39	~−18,000	~−33,500	~54
LG2C[b]	39	~−21,000	~−33,500	~63
LG2_nocap	39	~−18,000	~−32,700	~55
LG3_nocap	40	~−15,000	~−33,200	~45
LG2C_nocap	39	~−15,000	~−33,200	~45

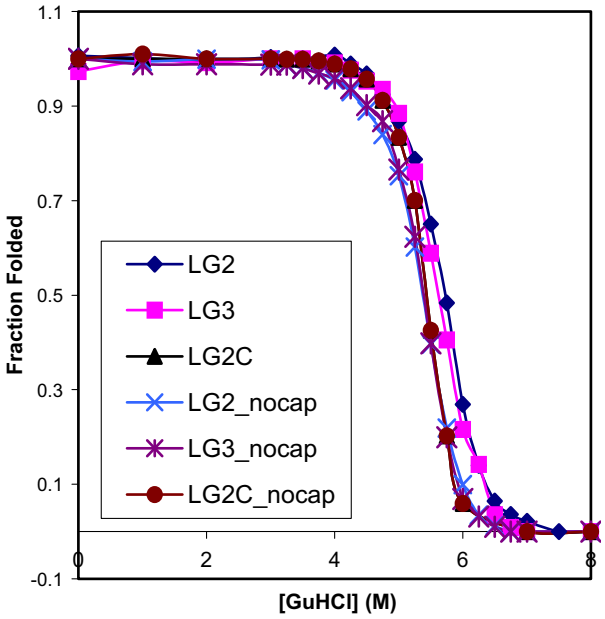

Fig. 4. Effect of GuHCl on the helicity ($[\theta]_{222}$) of the caviteins at ~40 μM in 50 mM pH 7.0 sodium-phosphate buffer at 20 °C.

Table 4
GuHCl-induced denaturation data calculated for the caviteins.

Cavitein	Concentration (μM)	$\Delta G^{o}_{H_2O}$ (kcal/mol)
LG2	39	−10.4 ± 0.3
LG2	4	−10.2 ± 0.3
LG3	39	−10.8 ± 0.4
LG3	4	−10.7 ± 0.4
LG2C	39	−11.8 ± 0.4
LG2C	3	−11.6 ± 0.3
LG2_nocap	39	−10.5 ± 0.4
LG2_nocap	3	−10.2 ± 0.4
LG3_nocap	40	−10.9 ± 0.4
LG3_nocap	4	−10.7 ± 0.3
LG2C_nocap	39	−11.2 ± 0.4
LG2C_nocap	4	−11.1 ± 0.4

structure. The presence of only 13 amide signals for these caviteins suggest that many of the amino acid residues are in a degenerate environment and therefore indistinguishable from each other, likely due to the fourfold symmetry of the cavitein.

The ^{1}H NMR spectra of LG2 and LG2_nocap and that of LG3 and LG3_nocap are similar. It is surprising that the signals in the ^{1}H NMR spectrum of LG2_nocap are sharper than comparable signals in LG2. The ^{1}H NMR spectrum of LG3 remains the sharpest of the caviteins, although still slightly less dispersed than LG2 and LG2_nocap. However, having a lower dispersion does not preclude a native-like structure, since it has been shown that coiled coil proteins generally exhibit less dispersion in the amide region than do square bundles [17]. Overall, the tertiary structures of the caviteins without caps are similar to the tertiary structures of their reference capped counterparts, since their ^{1}H NMR spectra comparable.

2.9. Hydrogen/deuterium amide exchange

Proteins have some conformational flexibility or dynamics. It is common to use NMR to study protein-amide protons that can be readily exchanged with solvent protons in aqueous media [18]. A representative stackplot of the ^{1}H NMR amide region for LG2_nocap is shown in Fig. 7. N-H/D exchange data were analyzed for all caviteins. The protection factors for the most protected proton for each cavitein are shown in Table 6.

The amide H/D exchanges of all of the capping caviteins were studied over the course of about 6 h depending on the cavitein. Many of the amide protons exchanged before the first scan could be acquired (~5 min) and are not likely involved in buried hydrogen bonds or are easily accessible to the solvent. However, a few amides were visible for a few hours, and their calculated protection factors are outlined in Table 6.

Table 6 shows that it is clear that the protons at ~8.5 ppm for LG2_nocap, LG3_nocap, and LG2C_nocap exhibit slightly less protection from exchange than the protons at ~8.5 ppm for LG2, LG3 and LG2C, respectively. It is possible that removal of the glycine cap may leave the hydrophobic core of the peptides slightly more exposed due to the unravelling of the helices, and hence more accessible to the solvent.

2.10. 1-Anilinonaphthalene-8-sulfonate (ANS) binding

ANS binding can be used as a diagnostic to probe the tertiary structures of proteins, with molten globule proteins generally binding ANS with a high affinity [19]. ANS binding was studied by fluorescence spectroscopy for the capping caviteins, and under standard experimental conditions [20] negligible binding was observed for all of the caviteins. The studies were completed using three different concentrations of 50, 100 and 150 μM per cavitein and negligible binding was observed (data not shown). Since all other four-helix bundle caviteins have exhibited negligible binding, it was not surprising that no ANS was found to bind to any of the caviteins studied [3].

3. Conclusions

Overall this work presents the design and synthesis of four-helix bundles containing peptides with and without N- and C-glycine caps. It was predicted that, if the glycine caps were indeed responsible for holding the tertiary structures intact, the caviteins lacking glycine capping residues would be less helical, less stable, and more dynamic than their capped counterparts, and would exhibit more molten globule-like characteristics. A reduction of 5–18% α-helicility for the uncapped caviteins together with their lower protections factors, compared to their capped counterparts, suggest that the capping residues do help hold the helix ends from unravelling. The uncapped caviteins although less α-helical,

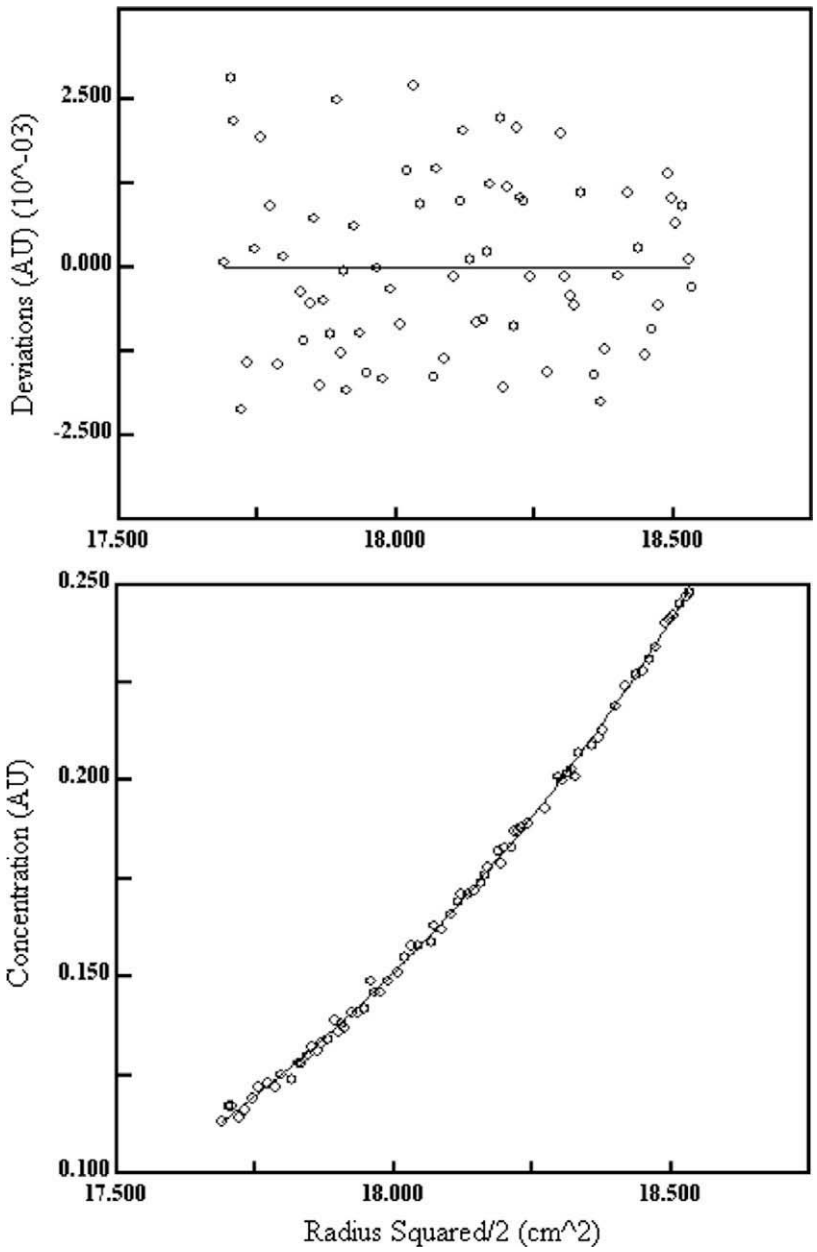

Fig. 5. Sedimentation equilibrium concentration distributions of LG2_nocap at a rotor speed of 27,000 rpm in 50 mM sodium-phosphate buffer, pH 7.0, 20 °C at 10 μM. In the lower panel the solid line represents a theoretical fit to a monomer equilibrium. The upper panel represents the residuals for the fit.

Table 5
Experimentally estimated molecular weights (MWs) determined by sedimentation equilibrium for the caviteins at 20 °C in 50 mM pH 7.0 sodium-phosphate buffer at concentrations of 10, 50 and 80 μM with rotor speeds of 27,000, 35,000 and 40,000 rpm.

Cavitein	Experimentally estimated MW (Da)	Calculated MW (Da)	Predominant species
LG2[a]	8500 ± 600	8016	Monomer
LG3[a]	8000 ± 300	8240	Monomer
LG2C[b]	8700 ± 600	8424	Monomer
LG2_nocap	8100 ± 400	7784	Monomer
LG3_nocap	8500 ± 500	8016	Monomer
LG2C_nocap	8300 ± 400	8200	Monomer

were of comparable stability to their capped counterparts, demonstrated by similar $\Delta G^{o}_{H_2O}$ values of unfolding. A slight difference in stability of ~0.3–2 kcal/mol for capping was expected depending on the helix termini. Furthermore, the caviteins with peptides linked to the cavitand template via their C-termini exhibited more molten globule-like characteristics than caviteins containing peptides linked via their N-termini. A crystal structure of a cavitein-dimer recently reported by Sherman and co-workers shows a stabilizing glycine C-capping interaction. This evidence further supports the rationale for including glycine C-caps in future cavitein designs [3g]. Therefore, capping residues will continue to be used as they help retain α-helicity, and help hold the tertiary contacts in place.

In the future, other amino acid residues apart from glycine could be studied to determine whether a more suitable capping residue exists. Furthermore, an optimization of the linker between the cavitand template and C-terminal linked peptides is necessary.

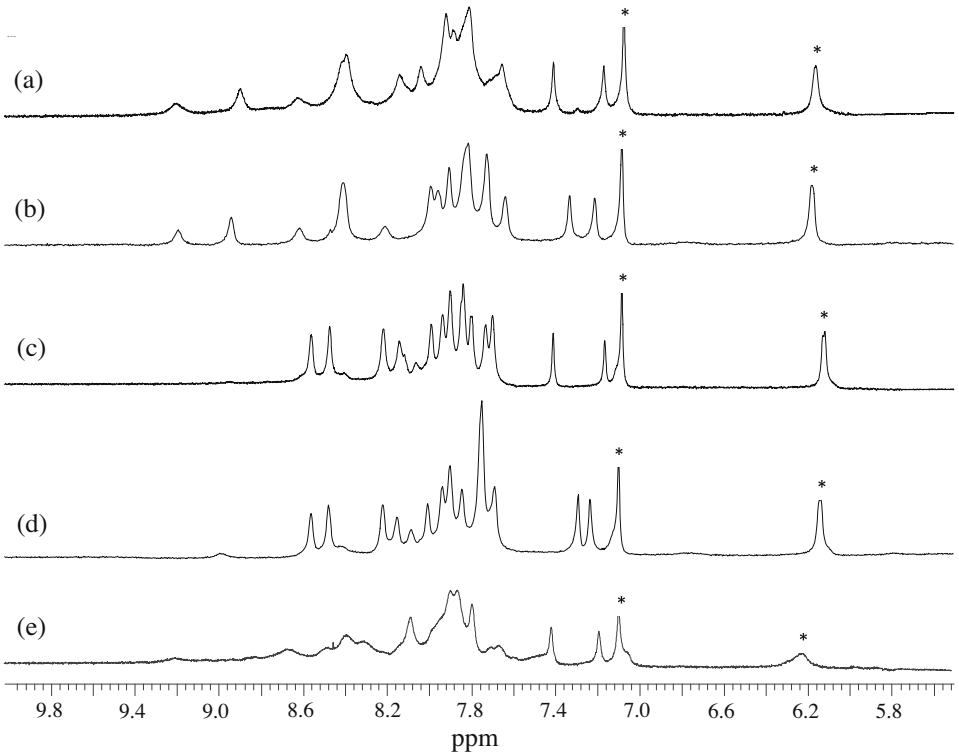

Fig. 6. Expansions of the amide regions of 500 MHz ^{1}H NMR spectra of the capping caviteins at ~1.5 mM in 10% D_2O, 45 mM sodium-phosphate buffer, pH 7.0 at 20 °C. (a) LG2 (b) LG2_nocap (c) LG3 (d) LG3_nocap (e) LG2C (∗ = cavitand signals).

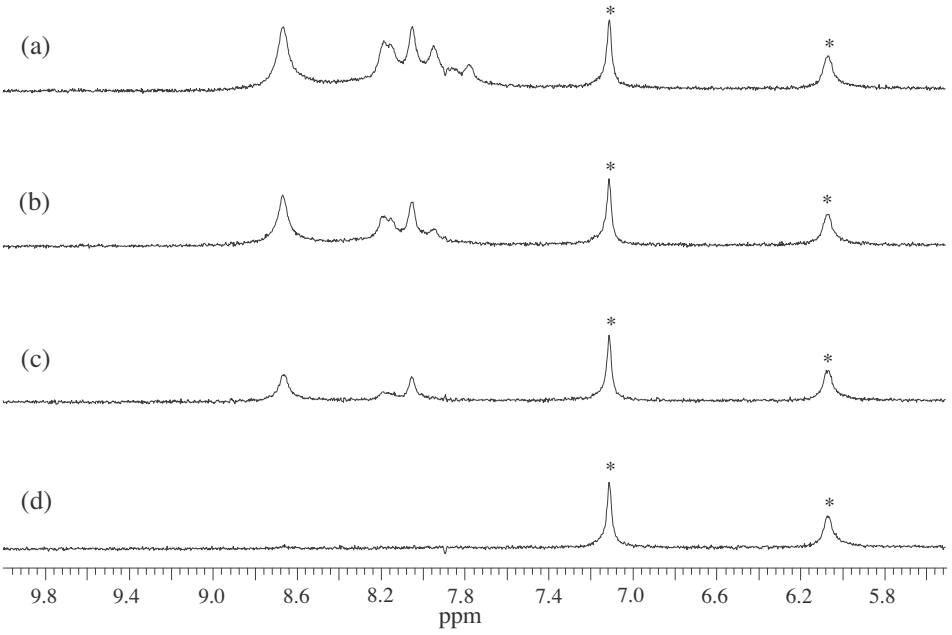

Fig. 7. Stackplot of 500 MHz ^{1}H NMR spectra illustrating the time dependent amide H/D exchange of LG2_nocap in 50 mM pD 5.02 $CD_3COOD/CD_3COO^-Na^+$ buffer at 20 °C. (a) 4 min (b) 18 min (c) 1 h 3 min (d) 6 h 9 min (∗ = cavitand signals).

4. Experimental

4.1. Cavitand synthesis

The synthesis of the arylthiol cavitand was synthesized following literature procedures [3a].

4.2. General

All reagents for the peptide and cavitein syntheses were reagent grade. The peptides and caviteins were purified by preparative reversed-phase HPLC using a Perkin–Elmer Biocompatible Pump 250 with a PE LC90 BIO Spectrophotometric UV detector and a KIPP and

Table 6
Data from the amide H/D exchange experiments of the caviteins in a 50 mM pD 5.02 $CD_3COOD/CD_3COO^-Na^+$ buffer at 20 °C.

Cavitein name	Amide proton chemical shift[a] (ppm)	First-order rate constant (h^{-1})	Half-life (h)	Protection factor [b]
LG2	8.5	3.37×10^{-2}	20	$(6.3 \pm 0.5) \times 10^3$
LG3	8.5	2.97×10^{-2}	23	$(7.3 \pm 0.5) \times 10^3$
LG2C	8.5	1.39	0.50	$(1.6 \pm 0.2) \times 10^2$
LG2_nocap	8.6	8.32×10^{-1}	0.80	$(2.6 \pm 0.3) \times 10^2$
LG3_nocap	8.6	1.67×10^{-1}	4.2	$(1.3 \pm 0.3) \times 10^3$
LG2C_nocap	8.5	2.08	0.33	$(1.0 \pm 0.2) \times 10^2$

[a] Only the data on the most protected proton is included.
[b] These values are based on the half-life of an unprotected proton at 20 °C at pD 5.02 to be 3.18×10^{-3} h.

ZONEN chart recorder. A Phenomenex Selectosil C_{18} reversed-phase HPLC column (preparative: 250 mm × 25 mm, 10 μM particle size, 300 Å pore size) was used. The wavelength for the UV detection was set at 229 nm for recognition of the amide chromophore. The samples were filtered through a 0.45 μM Nylon™ syringe filter (Phenomenex) prior to injection and run at a flow rate of 10 mL/min using helium sparged filtered water (0.1% TFA)/HPLC-grade acetonitrile (0.05% TFA) gradient. The purity of the peptides and caviteins were analyzed by analytical reversed-phase HPLC and were filtered prior to injection onto a Varian 9010 Pump with a Varian 9050 UV detector and a Varian 4290 Integrator. A Phenomenex Selectosil C_{18} reversed-phase HPLC column (analytical: 250 mm × 4.5 mm, 5 μM particle size, 100 Å pore size) was used. Analytical samples were run at a flow rate of 1 mL/min using the same solvents as for the preparative purification. The purified samples were evaporated *in vacuo* and lyophilized. The mass spectra were run on a MALDI-MS Bruker Biflex IV in reflectron mode using 50 μM cinnamic acid in 1:1, H_2O: MeCN, as a matrix. Cavitein concentrations were determined using a Bradford Assay [21] measured on a CARY UV–visible spectrophotometer. The pH's of the buffers were determined using a Fisher Scientific Accumet pH meter 915 calibrated with two purchased buffer standards (pH = 4.0 and 10.0).

4.3. Peptide synthesis

The peptides were synthesized following to a large extent literature procedures, with peptides **1** and **2** having previously been synthesized [3b,d]. The synthesis of lg2_nocap, and lg3_nocap followed similar experimental procedures as those described for lg2 and lg3. In the case of lg2c_nocap, the synthesis was identical to the synthesis of lg2c except that lg2c_nocap lacked an N-terminal glycine residue. The peptide synthesis involved using standard Fmoc techniques on an automated Applied Biosystems peptide synthesizer attached to an Apple IIsi MacIntosh computer. All Fmoc protected amino acids, solvents and coupling reagents were purchased from Advanced Chemtech (Louisville, KY, USA). The peptides were synthesized on a 0.25 mmol scale using the *FastMoc*™ protocols. Side chain protected amino acids were used for chemoselective synthesis of the peptide, which was in turn bound by its C-terminus to a resin developed by Rink [22] to afford a C-terminal amide upon cleavage. A single amino acid coupling cycle included a: (1) 13 min Fmoc deprotection using piperidine, (2) 6 min wash step using N-methylpyrrolidone (NMP), (3) 30 min coupling step to 1.0 mmol of the next Fmoc amino acid using 2-(1H-benzotriazole)1,1,3,3-tetramethyluronium hexafluorophosphate (HBTU) and 1-hydroxybenzotriazole (HOBt) as coupling reagent (note activation of the amino acid started with DIPEA), and lastly and (4) 6 min wash with NMP. NMP was the solvent throughout the synthesis with each cycle having an approximate time of 55 min.

Thereafter, chloroacetylation of the free N-terminus was achieved through manual treatment of the resin (600 mg peptide resin, ~300 mg peptide **1**, ~0.160 mmol) with chloroacetyl chloride (75 μL, 0.96 mmol, 6 equiv.) and DIPEA (165 μL, 0.95 mmol, 6 equiv.) in DMF for 1 h at room temperature under nitrogen. The last step included cleavage of the peptides from the resin in addition to removing the side chain protecting groups simultaneously using a 2 h treatment with 95% TFA/H_2O. An ice bath was used for the first 10 min of the reaction. After completion, the resin was removed by suction filtration through a medium frit filter with a CH_2Cl_2 wash. The TFA/CH_2Cl_2 filtrate was evaporated to a few mLs *in vacuo* and the crude peptide was precipitated using ice-cold diethyl ether. The peptide was recovered by suction filtration using a fine frit filter. The peptide was then dissolved in distilled water, filtered, and purified by reversed-phase HPLC. The peptide was lyophilized until a fluffy white solid peptide was obtained (105 mg, 23%).

Slight modifications to the above procedure were made for the preparation of peptides **3** and **6** (lg2c and lg2c_nocap) and are described for lg2c below. A C-terminal cysteine residue was added on the automated peptide synthesizer containing an S-trityl side chain protecting group. After peptide lg2c was removed from the automated peptide synthesizer the free N-terminus was acetylated through a manual treatment of lg2c (~300 mg resin, ~100 mg peptide **3**, ~0.6 mmol) with excess acetic anhydride (3.5 mL) in 1 mL NMP for 1 h at room temperature. The peptide resin was then filtered through a medium frit filter with DCM. The lg2c peptide was then cleaved off the resin and of protecting groups using a mixture of TFA (95%), H_2O (2.5%) and 1,2 ethanedithiol (2.5%). The last step involved activating the free C-terminus of lg2c by adding lg2c (20 mg, 10 μmol) in 3 mL ethanol to a rapidly stirring solution of 2,2′-dipyridyl disulfide (12 mg, 55 μmol) in 2 mL ethanol. The reaction was stirred at room temperature for 1 h. The ethanol was reduced to 1 mL *in vacuo*, and the solution was pipetted onto ice-cold diethyl ether. The resulting solid was re-dissolved in water (1.5 mL) containing 0.1% TFA, and filtered using a 0.45 μm nylon filter. Subsequent purification of lg2c by RP-HPLC and lyophilization afforded peptide **3** as a white solid (50 mg, 19%). All of the peptides were characterized for purity by the inspection of a single peak by analytical reversed-phase HPLC (>95% pure), and using MALDI-MS (see Table 7).

4.4. Cavitein synthesis

Caviteins **7**, **8**, **10** and **11** were synthesized by following literature procedures [3b]. The synthesis of cavitein **7** is described below, and similar procedures were followed for the synthesis of caviteins **8**, **10** and **11**. A solution of the arylthiol cavitand (1.1 mg, 1.4 μmol, 1 equiv.) and peptide **1** (21 mg, 11.3 μmol, 8 equiv.) were stirring in degassed DMF under N_2. DIPEA (2.5 μL, 15 μmol, 10 equiv.) was added in excess until the solution turned cloudy. The reaction was monitored (appearance of the cavitein peak) by analytical reversed-phase HPLC and was complete after 4 h. The crude reaction mixture was evaporated *in vacuo*, dissolved in water, filtered, and purified by reversed-phase HPLC to yield cavitein **7** as a fluffy white solid (5.5 mg, 49%) after lyophilization.

Table 7
% Yields and MALDI-MS Characterization of the "Activated" Peptides. (Note, calculated masses agreed within 1 Da).

Peptide	% Yield	Mass (Da.)
lg2[a]	85	1860
lg3[a]	82	1916
lg2c[b]	68	2037
lg2_nocap	78	1802
lg3_nocap	80	1860
lg2c_nocap	61	1980

The additional unwanted tris-cavitein byproduct was separated and removed during purification. The synthesis of caviteins **9** and **12** was very similar and followed literature procedures [12]. The caviteins were characterized using MALDI-MS and the masses are outlined in Table 8.

4.5. Circular dichroism (CD) spectroscopy

All CD spectra were recorded on a JASCO J-710 spectropolarimeter. The J-710 had a circulating water bath set to 25 °C, a 400 W xenon lamp, and an IBM-compatible PC computer for data acquisition. Some of the parameter settings include: 0.1 nm step resolution, 2 nm bandwidth, and 50 nm/min scanning speed. The J-710 spectropolarimeter was calibrated routinely using *d*-10-(+)-camphorsulfonic acid [23]. Each spectrum was an average of three scans subtracted from a reference background scan. Individual samples were run three different times to ensure reproducibility. The caviteins were monitored at 4 μM and 40 μM in 50 mM sodium-phosphate buffer (pH = 7.02) to check for concentration effects in a 1 cm and a 1 mm quartz cuvette, respectively.

The raw spectra were normalized to a mean residue ellipticity [θ] at 222 nm using the following equation:

$$[\theta]_{222} = \theta_{obs}/10lcn$$

where θ_{obs} is the observed ellipticity measured in millidegrees, l is the path length in cm, c is the cavitein concentration in mol/L, and n is the number of residues in the cavitein. Errors were on average ±5%.

Guanidine Hydrochloride (GuHCl) denaturation experiments were performed between 0 and 8.0 M GuHCl in a 50 mM sodium-phosphate buffered (pH = 7.0) cavitein solution. Data points were collected at 1 M units between 0 and 8.0 M to generate a rough unfolding curve. 0.25 interval denaturation studies were then completed to achieve accuracy in the unfolding region, and repeated three times to ensure reproducibility. Likewise, cavitein samples were monitored for unfolding at 4 μM and 40 μM to study concentration effects in a 1 mm and a 1 cm quartz cuvette, respectively. Samples were prepared immediately before data acquisition and equilibrated for 10 min (previously determined that any effect of GuHCl is immediate). The mean residue ellipticity was again monitored at [θ] = 222 nm.

Protein unfolding was analyzed using the linear extrapolation method of Santoro and Bolen [24]. According to this method, unfolding is a reversible, two-state process and that the free energy of folding is a linear function of the GuHCl concentration. The GuHCl denaturation data were fit using a nonlinear least-squares analysis to fit the pre-transitional baseline using the following equation:

$$\theta_{obs} = \theta_N(f_N)(1 - a[\mathrm{GuHCl}]) + \theta_U(1 - f_N)$$

where θ_{obs} is the mean residue ellipticity at 222 nm at a certain concentration of GuHCl, θ_N is the mean residue ellipticity of the folded state in the absence of GuHCl, θ_U is the mean residue ellipticity of the unfolded state, a is a constant and f_N is the fraction of the protein in the folded state. f_N is related to the free energy of unfolding, $\Delta G^o_{H_2O}$, by the following equation:

$$f_N = e^{((\Delta G^O H_2O - m[\mathrm{GuHCl}])/RT)}/[1 + e^{((\Delta G^O H_2O - m\mathrm{GuHCl}])/RT)}]$$

where $\Delta G^o_{H_2O}$ is the free energy of unfolding in the absence of GuHCl, m is the free energy change with respect to the concentration of GuHCl, R is the universal gas constant, and T is the temperature. A MacIntosh compatible computer program, KaleidaGraph V. 3.08d was used to calculate the values for $\Delta G^o_{H_2O}$ by a nonlinear least-squares regression analysis. The value of θ_N was normalized to one. The software analysis program calculated the reported errors.

4.6. Analytical ultracentrifugation (AUC)

Sedimentation equilibrium studies were carried out on a temperature-controlled Beckman Coulter Optima™ XL-I analytical ultracentrifuge. Sedimentation equilibrium experiments were run using either an An60 Ti rotor, or an An50 Ti rotor (four sample holders and eight sample holders, respectively) and a UV photoelectric scanner. A six sector cell, equipped with a 12 mm Epon centerpiece and quartz windows, was loaded with 3 × 120 μL of sample at three different concentrations made up in 50 mM sodium-phosphate buffer at pH = 7.0, and 3 × 130 μL of reference solvent. Data were collected at 20 °C and at rotor speeds of 27,000, 35,000, and 40,000 rpm until equilibrium was established. Samples were equilibrated for 40 h and single scans 3 h apart were overlaid to determine that equilibrium had been reached. Scanning parameters included: radial step size of 0.001 cm, step mode, 10 replicate scans, radial scan range between 5.8 cm and 7.3 cm, and UV detection at 270 nm. The solution density of the samples in sodium-phosphate buffer was taken to be 1.000 g/mL. The partial specific volumes of the caviteins were calculated based on their amino acid compositions [25].

The sedimentation equilibrium data was analyzed on a PC compatible software program called NONLIN [15]. This program uses a nonlinear least-squares analysis in order to generate a reduced molecular weight, σ, from which the actual experimental molecular weight, M, can be calculated. Nine sets of data (three different concentrations at the three different rotor speeds) per cavitein were analyzed at a time. The data were initially fit to a single non-associating ideal species model using the Lamm [26] equation below:

$$A_r = \mathrm{Exp}\,[\ln(A_o) + M\omega^2(1 - \bar{v}\rho/RT)(r^2 - r_o^2)] + E$$

where A_r is the absorbance at radius r, A_o is the absorbance at a reference radius r_o (the meniscus), M is the molecular weight in g/mol, ω is the angular velocity of the rotor in rad/s, $\bar{v}$ is the partial specific volume of the peptide, ρ is the density of the solvent in g/mL, R is the universal gas constant, T is the temperature in K, and E is the baseline correction factor or baseline offset. For the NONLIN fitting details see the supporting information.

Table 8
% Yields and MALDI-MS characterization of the Caviteins made from "Activated" peptides (note, calculated masses agreed within 1 Da).

Cavitein	% Yield	Mass (Da.)
LG2[a]	29	8016
LG3[a]	34	8240
LG2C[b]	32	8424
LG2_nocap	33	7784
LG3_nocap	31	8016
LG2C_nocap	25	8200

4.7. ^{1}H NMR spectroscopy

The 1D ^{1}H NMR spectra were run at 20 °C on a 500 MHz Varian Unity instrument, and the samples were dissolved in 45 mM sodium-phosphate buffer at pH = 7.0 (90:10, H_2O:D_2O) to a final concentration of approximately 1.5 mM. Spectra were processed using a PC "Windows XP" compatible NMR processing program, MestReC 2.3.

The 1D ^{1}H NMR N-H/D exchange spectra were run at 20 °C, and the samples were prepared as follows: ~1.5 mM cavitein solutions in a 50 mM acetic acid/acetate buffer at pH = 4.62 were lyophilized to a white solid. D_2O was then added to the lyophilized samples in the NMR room to the previous volume before lyophilization of 0.5 mL. The resulting sample in a deuterated acetic acid/acetate buffer at pD = 5.02 was transferred quickly to an NMR tube. The pH was re-checked after the exchange experiments were completed to ensure a correct reading of pD = 5.02, since pH has a dramatic effect on exchange rates. The pD was corrected for isotope effects using the equation [27]:

$$pD = pH_{\text{read}} + 0.4$$

where pH_{read} is the reading of the pH electrode. The first scan was acquired 5 min after the addition of D_2O and subsequent scans were collected at various time intervals until all of the amide protons had completed exchanged with deuterium. The spectra were analyzed using the same processing program mentioned above. The peak heights were integrated and normalized with the non-exchangeable cavitand proton (H_{out}) at ~6.1 ppm. The first-order rate constants were calculated using the first-order rate equation:

$$\ln([Ho]/[Ht]) = k_{obs}t$$

where k_{obs} is the first-order rate constant, t is the time at which the scan was taken, $[H_o]$ is the integration of the proton at time zero, and $[H_t]$ is the integration of the same proton at time t. The half-lives, $t_{1/2}$, of the amide protons were then calculated using the equation:

$$t_{1/2} = \ln 2/k_{obs}$$

Protection factors were then calculated using the equation:

$$P = k_{int}/k_{obs}$$

where P is the protection factor, k_{obs} is the experimental first-order rate constant, and k_{int} is the first-order rate constant for an "unprotected" amide proton at pH = 4.62 at 20 °C. k_{int} can be calculated from the intrinsic half-life, $t_{1/2-\text{int}}$, which is determined using the following equation [18a]:

$$T_{1/2\text{-}int} = 200/[10^{(pH-3)} + 10^{(3-pH)}][10^{0.05T}]$$

where $t_{1/2\text{-}intrinsic}$ is the intrinsic half-life for an unprotected proton, and T is the temperature in °C. Errors represent one standard deviation from three rate constant estimates.

4.8. ANS binding

ANS fluorescence measurements were made on a Varian CARY Eclipse Fluorescence Spectrophotometer equipped with a Xenon Arc lamp. Samples were run at 20 °C using a 1 cm path length with concentrations of 50 μM and 100 μM, and contained 2 μM ANS respectively, in 50 mM sodium-phosphate buffer at pH = 7.02. Reference emission spectra were collected for 95% ethanol and 100% HPLC-grade methanol with 2 μM ANS. Excitation was at 370 nm and emission was recorded between 385 and 600 nm.

Acknowledgments

I would like to thank the Natural Sciences and Engineering Research Council of Canada for its financial support. I would also like to thank M. Okon for acquiring the ^{1}H NMR spectra and sharing his expertise in protein NMR. Additional acknowledgements are given to The Center for Biothermodynamics and support from the Michael Smith Foundation for Health Research for data obtained on the AUC, and to F. Rosell and G. Mauk for the use of their Varian CARY Eclipse Spectrophotometer in the Life Sciences Center.

References

[1] (a) W.F. Degrado, Adv. Prot. Chem. 39 (1988) 51–124;
(b) M.H. Hecht, J.S. Richardson, W.F. DeGrado, Biochemistry 36 (1997) 2450–2458;
(c) P.B. Harbury, J.J. Plecs, B. Tidor, T. Alber, P.S. Kim, Science 282 (1998) 1462–1467;
(d) L. Baltzer, H. Nilsson, J. Nilsson, Chem. Rev. 101 (2001) 3153–3163.
[2] (a) M. Mutter, S. Vuilleumier, Angew. Chem. Int. Ed. Engl. 28 (1989) 535–554;
2b M. Mutter, Trends Biochem. Sci. 13 (1988) 260–265.
[3] (a) B.C. Gibb, A.R. Mezo, A.S. Causton, J.R. Fraser, F.C.S. Tsai, J.C. Sherman, Tetrahedron 51 (1995) 8719–8732;
(b) A.R. Mezo, J.C.J. Sherman, Am. Chem. Soc. 121 (1999) 8983–8994;
(c) A.S. Causton, J.C.J. Sherman, Pep. Sci. 6 (2002) 275–282;
(d) H.E.K. Huttunen-Hennelly, J.C. Sherman, Pept. Sci. 1 (2008) 37–50;
[3e] H.E.K. Huttunen-Hennelly, J.C. Sherman, Org. Biomol. Chem. 5 (2007) 3637–3650;
(f) E.S. Seo, W.R.P. Scott, S.K. Straus, J.C. Sherman, Chem. Eur. J. 13 (2007) 3596–3605;
(g) J.O. Freeman, W.-C. Lee, M.E.P. Murphy, J.C.J. Sherman, Am. Chem. Soc. 131 (2009) 7421–7429.
[4] (a) V. Nanda, M.M. Rosenbkatt, A. Osyczka, H. Kono, Z. Getahun, P.L. Dutton, J.G. Saven, W.F.J. DeGrado, Am. Chem. Soc. 127 (2005) 5804–5805;
(b) J. Brask, J.M. Dideriksen, J. Nielsen, K.J. Jensen, Org. Biomol. Chem. 4 (2003) 306–318;
(c) W.F. DeGrado, Z.R. Wasserman, J.D. Lear, Science 243 (1989) 622–628;
(d) M.H. Hecht, J.S. Richardson, D.C. Richardson, R.C. Ogden, Science 249 (1990) 884–891;
(e) O. Nyanguile, M. Mutter, G. Tuchscherer, Pept. Sci. 1 (1994) 9–16.
[5] (a) J. Kaplan, W.F. DeGrado, Proc. Natl. Acad. Sci. USA 101 (2004) 11566–11570;
(b) J.M. Mason, K.M. Arndt, Chem. Biochem. 5 (2004) 170–176;
(c) Pinto, G.R. Dieckmann, C.S. Ghandi, C.G. Papworth, J. Braman, M.A. Shaughnessy, J.D. Lear, R.A. Lamb, W.F. DeGrado, Proc. Natl. Acad. Sci. USA 94 (1997) 11301–11306;
(d) J.D. Lear, H. Gratkowski, W.F. DeGrado, Biochem. Soc. Trans. 29 (2001) 559–564;
(e) P. Rossi, L. Tecilla, P. Baltzer, Chem. Eur. J. 10 (2004) 4163–4170;
(f) W.F.J. DeGrado, Am. Chem. Soc. 119 (1997) 3212–3217;
H.K. Rau, N. DeJonge, W. Haehnel, Proc, Natl Acad. Sci. USA 95 (1998) 11526–11531.
[6] L. Pauling, R.B. Corey, H.R. Branson, Proc. Natl. Acad. Sci. USA 37 (1951) 205–210.
[7] (a) A.J. Doig, M.W. Macarthur, B.J. Stapley, J.M. Thornton, Prot. Sci. 6 (1997) 147–155;
(b) R. Aurora, G.D. Rose, Prot. Sci. 7 (1998) 21–38;
(c) A.J. Doig, R.L. Baldwin, Prot. Sci. 4 (1995) 1325–1336.
[8] S. Marqusee, R.L. Baldwin, Proc. Natl. Acad. Sci. USA 84 (1987) 8898–8902.
[9] (a) S. Padmanabhan et al., Nature 344 (1990) 268–270;
(b) G. Merutka, E. Stellwagen, Biochemistry 29 (1990) 894–898.
[10] L.G. Presta, G.D. Rose, Science 240 (1988) 1632–1641.
[11] B.C. Gibb, A.R. Mezo, J.C. Sherman, Tetrahedron Lett. 36 (1995) 7587–7590.
[12] A.S. Causton, J.C. Sherman, Bioorg. Med. Chem. 7 (1999) 23–27.
[13] (a) W.C. Johnson Jr., Proteins Struc. Func. Genet. 7 (1990) 205–214;
(b) R.W. Woody, Methods Enzymol. 246 (1995) 34–70.
[14] J.C. Hansen, J. Lebowitz, B. Demeler, Biochemistry 33 (1994) 13155–13163.
[15] M.L. Johnson, J.J. Correia, D.A. Yphantis, H.R. Halvorson, Biophys. J. 36 (1981) 575–588.
[16] K.N.M.R. Wüthrich, Of Proteins and Nucleic Acids, Wiley, New York, 1986.
[17] (a) R. Wiltscheck, R.A. Kammerer, S.A. Dames, T. Schulthess, M.J. Blommers, J. Engel, A.T. Alexandrescu, Prot. Sci. 6 (1997) 1734–1745;
(b) N.J. Greenfield, G.T. Montelione, R.S. Farid, S.E. Hitchcock-DeGregori, Biochemistry 37 (1998) 7834–7843.
[18] (a) S.W. Englander, N.W. Downer, H. Teitelbaum, Annu. Rev. Biochem. 41 (1972) 903–905;
(b) T.M. Raschke, S. Marqusee, Curr. Opin. Biotech. 9 (1998) 80–86;
(c) S.W. Englander, L. Mayne, Y. Bai, T.R. Sosnick, Protein Sci. 6 (1997) 1101–1109;
(d) M.-F. Jeng, S.W. Englander, G.A. Elove, A.J. Wand, H. Roder, Biochemistry 29 (1990) 10433–10437;
(e) F.M. Hughson, P.E. Wright, R.L. Baldwin, Science 249 (1990) 1544–1548.

[19] K. Kuwajima, Proteins Struct. Funct. Genet. 6 (1989) 87–103.
[20] (a) S. Roy, G. Ratnaswamy, J.A. Boice, R. Fairman, G. McLendon, M.H.J. Hecht, Am. Chem. Soc. 119 (1997) 5302–5306;
(b) D.P. Raleigh, S.F. Betz, W.F.J. DeGrado, Am. Chem. Soc. 117 (1995) 7558–7559.
[21] M.M. Bradford, Anal. Biochem. 72 (1976) 248–254.
[22] H. Rink, Tetrahedron Lett. 28 (1987) 3787–3790.
[23] G.C. Chen, J.T. Yang, Ana. Lett. 10 (1977) 1195–1207.
[24] (a) M.M. Santoro, D.W. Bolen, Biochemistry 27 (1988) 8063–8068;
(b) M.M. Santoro, D.W. Bolen, Biochemistry 31 (1992) 4901–4907.
[25] E.J. Cohn, J.T. Edsall, Amino Acids, Peptides and Proteins as Ions and Dipolar Ions, Reinhold Publishing Corporation, New York, 1943.
[26] Lamm, O. Die Differentialgleichung der Ultrazentrifugierung. Ark. Mat. Astr. Fys. 1929, 21B, 1–4 [in german].
[27] P.K. Glasoe, F.A. Long, J. Phys. Chem. 64 (1960) 188–190.